AIAA JOURNAL
Vol. 35, No. 1, January 1997

Prediction of Strongly Curved Turbulent Duct Flows with Reynolds Stress Model

Jiang Luo* and Budugur Lakshminarayana†
Pennsylvania State University, University Park, Pennsylvania 16802-1400

The effects of strong convex and concave curvature on turbulent duct flows are investigated. A compressible Navier–Stokes code incorporating Reynolds stress models has been developed using a four-stage Runge–Kutta scheme. Numerical computations have been carried out for strongly curved 180-deg turnaround duct flows with a Reynolds stress model, an algebraic Reynolds stress model, and a nonlinear k-ε model. A detailed assessment of the models' capability in predicting the effects of strong streamline curvature has been carried out. It is observed that the Reynolds stress model provides the best predictions for major features of this highly curved duct flow, including strong enhancement of turbulence near the concave wall, complete damping of turbulence near the convex wall, and the subsequent separation downstream of the bend. It is also found that the modeling of the concave curvature effect is different from the modeling of the convex curvature effect, even qualitatively. The effect of curvature parameter δ/R on the development of mean flow and turbulence has been examined by numerical simulations with the Reynolds stress model.

Nomenclature

C_f	= skin-friction coefficient, $\tau_w/(0.5\rho U_m^2)$
C_p	= wall static pressure coefficient, $(P - P_{\text{inlet}})/(0.5\rho U_m^2)$
H	= duct height
k	= turbulent kinetic energy
P	= static pressure
P_{ij}	= production rate of Reynolds stress
P_k	= production rate of turbulent kinetic energy
R	= curvature radius, $0.5/1.5H$ for inner/outer wall
Re	= Reynolds number, $U_m H/\nu$
r	= radial coordinate
S	= coordinate along duct centerline ($S = 0.0$ at bend entrance)/invariant of strain rate ($S^2 = 2S_{ij}S_{ij}$)
U	= longitudinal mean velocity
U_m	= bulk velocity
u, v, w	= fluctuating velocities in streamwise, normal (radial), and cross-stream directions
$\overline{u_i u_j}$, $\langle u_i u_j \rangle$	= Reynolds stress
x	= longitudinal coordinate, $x < 0.0$ upstream, $x > 0.0$ downstream of bend, $x = 0.0$ at entrance and exit of bend
y	= coordinate normal to wall (positive from inner wall to outer wall)/normal distance from wall
y^+	= wall distance variable, yu_τ/ν
δ	= boundary-layer thickness
ε	= dissipation rate of turbulent kinetic energy
θ	= angle into bend measured from bend entrance/tangential coordinate
ν, ν_t	= laminar and turbulent kinematic viscosity
τ_w	= wall shear stress

Introduction

THE effects of streamline curvature on turbulent flows are significant in many engineering applications because they have been found to be surprisingly large, usually being an order of magnitude greater than that suggested by the additional terms in the flow equations, as pointed out by Bradshaw.[1] Many of the experimental data reveal that the turbulent shear stress is largely damped on highly convex curved surfaces (e.g., Ref. 2). On the contrary, the turbulence has been observed to be amplified greatly by concave curvature (Ref. 3). There have been many computational efforts to model curved turbulent shear flows. To predict the stabilizing and destabilizing curvature effects, it is necessary to adopt empirical modifications to eddy viscosity models.[1] On the other hand, direct solutions of Reynolds stress transport equations by Gibson et al.[4] and others have indicated that the Reynolds stress model (RSM) can account for the effects of curvature without empirical modifications.

Sandborn and Shin[5] and Monson et al.[6] recently carried out detailed measurements for a planar U-duct flow, which closely represents major features of the flow in the annular turnaround ducts of the powerhead on the Space Shuttle main engine. The curvature parameter δ/R is on the order of $O(1)$, being significantly higher than those in the previous measurements. With strong convex and concave curvature effects and extensive separation from the convex surface, this duct flow represents a major challenge for turbulence modelers. Computations with different variants of eddy viscosity models[6–9] have not been satisfactory, indicating the need for higher-order turbulence models, such as the RSM. However, most predictions of curved flows with the RSM have been obtained with boundary-layer codes. Thus they are limited to predicting thin shear layers with mild curvature and/or convex curvature. The effects of strong concave curvature and convex curvature (and subsequent separation) have not been fully investigated with differential RSM models.

The objective of this paper is to develop a Navier–Stokes procedure incorporating Reynolds stress models; to predict strongly curved duct flows and to assess the performance of the RSM, the algebraic Reynolds stress model, and a nonlinear k-ε model; and to examine the effects of δ/R on the mean flow and turbulence quantities inside the bend.

Turbulence Models

A brief description of the turbulence models incorporated into the numerical procedure are given next. More detailed descriptions are given in Luo and Lakshminarayana.[10]

The RSM model employed in the present study is the same as the widely used Reynolds stress model of Gibson and Launder[11] except for the diffusion term. The turbulent diffusion term is modeled using a simple isotropic stress diffusion model. This model is

Received May 11, 1995; presented as Paper 95-2241 at the AIAA 26th Fluid Dynamics Conference, San Diego, CA, June 9–12, 1995; revision received July 2, 1996; accepted for publication Aug. 23, 1996; also published in *AIAA Journal on Disc*, Volume 2, Number 1.

*Ph.D. Candidate, Department of Aerospace Engineering; currently Senior Engineer, Solar Turbines, Inc., San Diego, CA 92101. Student Member AIAA.

†Evan Pugh Professor, Department of Aerospace Engineering, and Director, Center for Gas Turbines and Power, 153 Hammond Building. Fellow AIAA.

adopted because Lien and Leschziner[12] found that it provided better prediction of the reattachment process than the generalized gradient diffusion hypothesis for separated flows. This model is given by

$$D_{ij} = \frac{\partial}{\partial x_k}\left[C_s \frac{k^2}{\varepsilon}\left(\frac{\partial \overline{u_i u_j}}{\partial x_k} \right) \right] \tag{1}$$

By assuming the convective and diffusive transport of individual Reynolds stress components are locally proportional to the transport of turbulent kinetic energy,[13] the differential equations in the RSM can be simplified to nonlinear algebraic equations, resulting in the algebraic Reynolds stress model (ARSM), which is more economical than the RSM model. The k and ε required in the ARSM are obtained from the standard k-ε model.[14] Many applications of the ARSM model to the flows with mild curvature and rotation effects can be found in Lakshminarayana.[15]

The Reynolds stress algebraic equation model developed by Shih et al.[16] is one of the latest nonlinear k-ε models (denoted as NL k-ε model hereafter). The motive for incorporating this model is to compare it with the ARSM, because these two models are similar in some aspects. However, there is significant difference between them. Unlike the ARSM, the NL k-ε model does not include the modeling for the pressure–strain correlation, which is responsible for the redistribution of turbulent kinetic energy and plays a dominant role in the evolution of the flow.

Since all of the preceding models are based on high Reynolds number assumption, they cannot be integrated down to the wall. For all of the models used in the present study, the near-wall region is handled by a one-equation model originally developed by Wolfshtein[17] and modified by Chen and Patel.[18] The matching location is at fixed grid lines with $y^+ \approx 70$. More details on the matching are given in Luo and Lakshminarayana.[10]

Numerical Procedure

A Navier–Stokes procedure, incorporating various turbulence models described earlier, has been developed based on the code due to Kunz and Lakshminarayana.[19] The equations are integrated in time by an explicit four-stage Runge–Kutta scheme. The convection and diffusion terms are discretized on a nonstaggered grid using second-order accurate central differencing. Fourth-order and second-order artificial dissipation terms (with coefficients around 0.02 and 0.25)[19] are included to damp high wave number errors and to improve the shock capturing, respectively. Eigenvalue scaling and the local velocity scaling [using $(U/U_m)^2$] of artificial dissipation terms are used to avoid contamination of the solution by artificial dissipation.

For the present two-dimensional flow, only the equations for $\langle uu \rangle$, $\langle vv \rangle$, $\langle ww \rangle$, and $\langle uv \rangle$ are solved. These equations are discretized in space and integrated in time in the same way as the mean flow equations. A second-order artificial dissipation term is added to the Reynolds stress transport equations to prevent odd-even decoupling, because the convection terms are also discretized with central differencing. The required value of artificial dissipation for convergent solution is fairly small (with the coefficient around 0.02 for second-order smoothing). Local velocity scaling is also used. The artificial dissipation coefficient in the normal direction is taken as a small fraction (e.g., $\frac{1}{10}$) of that in the streamwise direction, which further reduces the influence of smoothing on the convergent solution to a negligible level. The iteration of the RSM equation in the present time-marching procedure is found to be stable, without the implementation of elaborate stabilizing measures such as those required for pressure-based methods.[20] Sotiropoulos and Patel[21] have made similar observation in their computation of a transition duct flow using a low Reynolds number RSM model with an explicit Runge–Kutta scheme.

Results and Discussion

Sandborn and Shin[5] carried out detailed measurement of the flow in a two-dimensional turnaround-duct water tunnel with $Re = 2.2 \times 10^5$. Monson et al.[6] measured the flow in a similar turnaround duct with air at $Re = 1 \times 10^6$. These two cases are computed in this paper. The geometry and grid of the duct are shown in Fig. 1, where every other grid line is plotted. Grid-independent solutions are obtained by using 251×141 (streamwise $\times$ normal) and 291×141 grids for the Sandborn and Shin[5] duct and the Monson et al.[6] duct, respectively. A systematic grid independence study has been performed. For the Monson et al. duct, predictions using other grids, such as the 251×121 grid, are found to be very close to those from the 291×141 grid except in the separated flow region. Further refinement of the grid (e.g., 321×161) results in negligible difference in the final solution. Similar observation has also been made for the Sandborn and Shin duct. Fine grids are used here to minimize the truncation errors in the separated flow region. The first grid point near the wall is located around $y^+ = 1$. The profiles for streamwise velocity, four Reynolds stress components, and dissipation rate are specified at the inlet. For each case, the inlet boundary conditions were obtained by computation of the developing flow in a long straight channel with the corresponding Reynolds number. This method provided inlet conditions that agree with the data very well.[10]

Convergence criteria are taken as four decades drop of rms density residual and 2.5–3 decades drop of the rms residual for ε. The difference between the computed mass flow rate at the inlet and at the exit is less than 0.2% of the inlet mass flow rate. The CPU time required by the RSM and the ARSM is about 250 and 70%, respectively, more than that of the standard k-ε model. For the NL k-ε model, the required CPU time is typically 30% more than that of the standard k-ε model.

Mean Velocity and Turbulence Properties Inside the 180-deg Bend

The two cases described earlier have not only different Reynolds numbers but also different values of the curvature parameter δ/R. For the Monson et al.[6] case, δ/R are about 0.7 and 0.2, for boundary layers at $x \approx -1H$ on the convex and concave walls, respectively, whereas for the Sandborn and Shin[5] case, corresponding values of δ/R are about 1.0 and 0.3. The predictions at $\theta = 0$, 30, 90, and 180 deg and $2H$ for Monson et al.[6] ($Re = 10^6$) are presented in this section. To highlight the performance of the three anisotropic models, predictions by the standard k-ε model are also included for comparison.

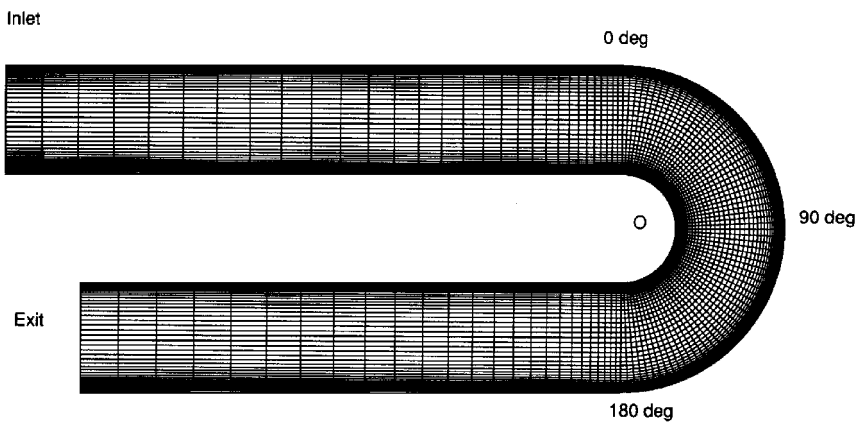

Fig. 1 Duct geometry and grid.

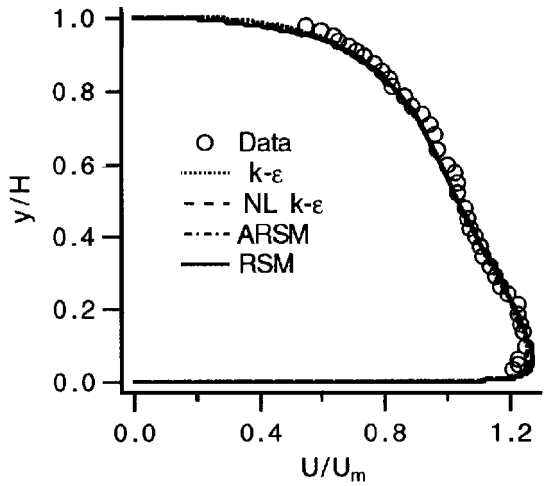

a) Longitudinal velocity

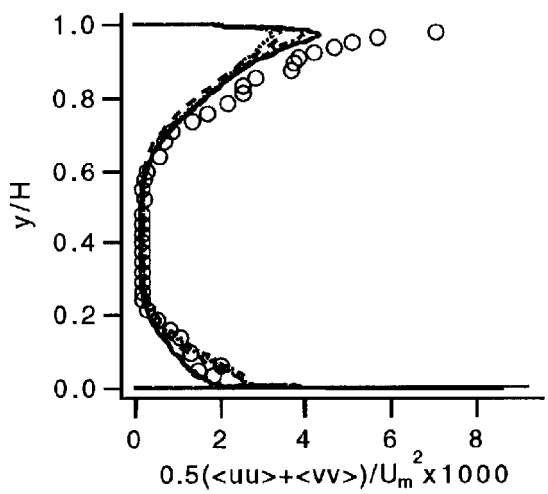

b) Turbulent kinetic energy

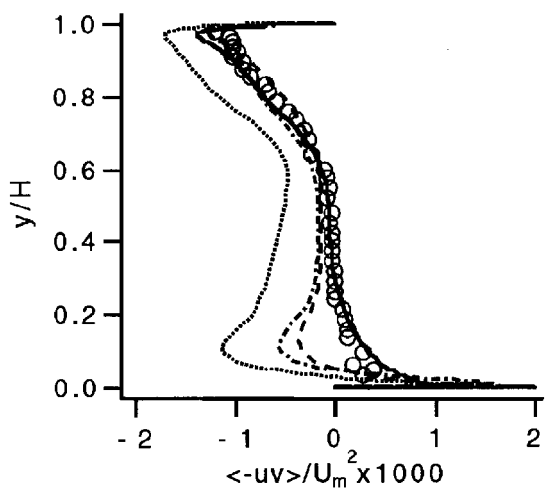

c) Turbulent shear stress

Fig. 2 Profiles at $\theta = 0$ deg (data by Monson et al.,[6] $Re = 1 \times 10^6$).

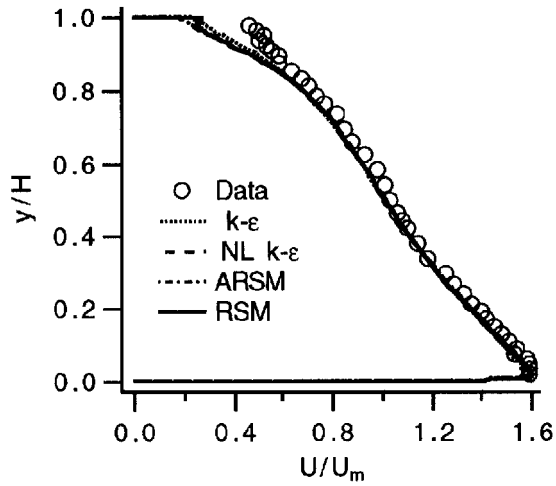

a) Longitudinal velocity

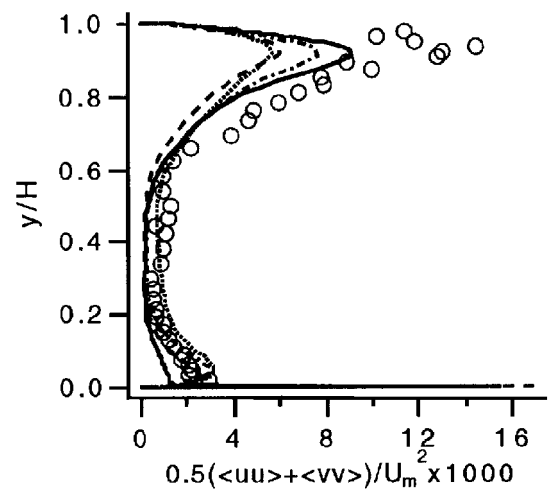

b) Turbulent kinetic energy

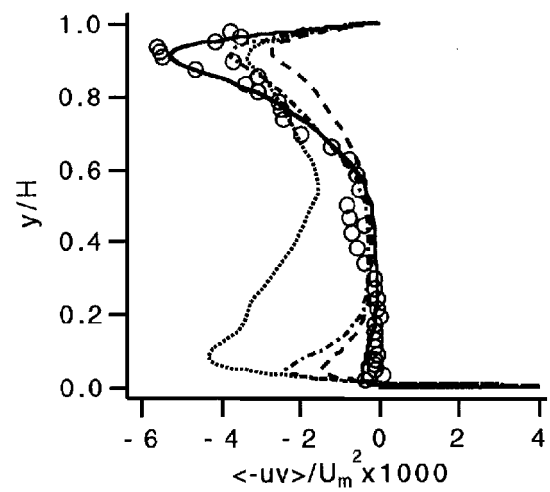

c) Turbulent shear stress

Fig. 3 Profiles at $\theta = 30$ deg (data by Monson et al.,[6] $Re = 1 \times 10^6$).

The predicted profiles of U, $\frac{1}{2}(\langle uu \rangle + \langle vv \rangle)$, which is referred to as turbulent kinetic energy in the following for brevity, and $\langle -uv \rangle$ at $\theta = 0$ deg are shown in Figs. 2a–2c, respectively. The mean velocity profiles predicted by all of the models are in excellent agreement with the data. The flow is undergoing rapid acceleration near the inner wall and deceleration near the outer wall. The curvature effects on turbulence can be clearly observed in Figs. 2b and 2c. The convex curvature, as well as large flow acceleration, strongly attenuates the turbulence shear stress and the kinetic energy near the inner wall. All of the four models yield similar predictions for the turbulent kinetic energy. In Fig. 2c, all of the three anisotropic models provide good predictions for $\langle -uv \rangle$ near the concave wall. Near the convex wall, however, only the RSM predicts the correct sign and magnitude of $\langle -uv \rangle$. Other models not only predict the wrong sign for $\langle -uv \rangle$ but also significantly overpredict the magnitude.

As the flow reaches $\theta = 30$ deg, the turbulence has been greatly damped near the convex wall and the measured shear stress is close to zero over a large region (Figs. 3b and 3c). On the other hand, large amplification of turbulence is observed near the concave wall. The Reynolds stress model captures both these features very well. The k-ε model fails to account for the curvature effect and predicts nearly symmetric profile of shear stress $\langle -uv \rangle$, which is much higher than

the data near the convex wall but lower than the data near the concave wall. The prediction of the ARSM model lies between those of the RSM model and the k-ε model. Overall, the ARSM prediction is close to that of the RSM model and is much better than that of the k-ε model, indicating that the error caused by the basic assumption in the ARSM is not significant for the flows inside bend, where the transport terms are known to be small in the balance of budget.

The NL k-ε model predicts low turbulence near the convex wall (Figs. 3b and 3c); indeed, its prediction of $\langle -uv \rangle$ is slightly better than that of the ARSM model. However, unlike the ARSM, the NL k-ε model predicts a reduced level of turbulence near the concave wall, which is opposite to the experimental observation. This surprising behavior is due to the fact that the NL k-ε model's mechanism for capturing the reduction of turbulence is very different from those of the Reynolds stress closures. Unlike the stress models, the NL k-ε model predicts weak anisotropy of turbulence, and its performance is mainly dependent on the variation of the coefficient C_μ in eddy viscosity formulation, as reported by Shih et al.[16] The reduced turbulent energy and shear stress predicted by this model are largely due to the reduced value of C_μ, which is a function of the parameter $\eta(Sk/\varepsilon)$. The value of C_μ is much lower than the standard value of 0.09 in flow regions with large strain rate, such as near the convex wall, and in regions with high value of k/ε, such as near the concave wall.

The phenomenological behavior of the turbulence and the performance of the stress models and the eddy-viscosity models for predicting the curvature effects on turbulence can be understood, qualitatively, by examining the formulation for the production term in these equations. For flows in curved ducts with constant radius, it is more convenient to express the velocity gradient in cylindrical-polar coordinates (r, θ). For an isotropic eddy viscosity model, neglecting second-order small terms, the production rate of turbulent kinetic energy is given by

$$P_k = \nu_t \left(\frac{\partial U_\theta}{\partial r} - \frac{U_\theta}{r} \right)^2 + 4\nu_t \left(\frac{1}{r} \frac{\partial U_\theta}{\partial \theta} \right)^2 \tag{2}$$

whereas in the stress models the production terms are exact. Neglecting second-order small terms, the production rates of turbulent kinetic energy and shear stress are given by

$$P_{\theta\theta} + P_{rr} = -2\overline{u_r u_\theta} \left(\frac{\partial U_\theta}{\partial r} - \frac{U_\theta}{r} \right) - 2(\overline{u_\theta^2} - \overline{u_r^2}) \left(\frac{1}{r} \frac{\partial U_\theta}{\partial \theta} \right) \tag{3}$$

$$P_{r\theta} = -\overline{u_r^2} \frac{\partial U_\theta}{\partial r} + \overline{u_\theta^2} \frac{U_\theta}{r} \tag{4}$$

Following Launder et al.,[22] to highlight the interaction between the stress and the strain in curved flows, it is helpful to consider two simple strain fields with curvature effects: free-vortex motion $U_\theta = A/r$ (approximately representing the flow over a concave wall with velocity decreasing with radius inside the viscous layer) and solid-body rotation $U_\theta = \omega r$ (approximately representing the flow over a convex wall with velocity increasing with radius inside the viscous layer). For the free-vortex type flow, the production rates in the stress closures are given, respectively, by

$$P_{r\theta} = (\overline{u_\theta u_\theta} + \overline{u_r u_r})\, A/r^2 \tag{5a}$$

$$P_{\theta\theta} + P_{rr} = 4\overline{u_r u_\theta}\, A/r^2 \tag{5b}$$

Equation (5) indicates that an increase in $\overline{u_r u_\theta}$ causes a rise in $(P_{rr} + P_{\theta\theta})$, which leads to an increase in $(\overline{u_\theta u_\theta} + \overline{u_r u_r})$. The production rate $P_{r\theta}$ is thus increased and so is the shear stress. Such an interaction will lead to successive amplification of turbulent energy and shear stress. For solid-body rotation, $(P_{rr} + P_{\theta\theta})$ is equal to zero. Hence, the production of turbulent energy and shear stress is suppressed. Therefore, exact production terms in the stress closures are capable of capturing the strong interaction between individual stress and the streamline curvature, which cannot be represented by Eq. (2). Nevertheless, the first term on the right-hand side of Eq. (2) does decrease in convex curved flows and increase in concave curved flows. Thus the k-ε model should be able to capture some effects of curvature. But the k-ε model still predicts an excessive level of turbulence near the convex wall, which is actually caused by the second term of Eq. (2).

Large streamwise velocity gradients $(\partial U_\theta/\partial\theta)$ often exist in strongly curved flows, as in the present case. Consider Eq. (3); the streamwise component Reynolds stress $\overline{u_\theta u_\theta}$ is larger than the normal component $\overline{u_r u_r}$ at the bend entrance. Thus, a positive gradient of streamwise velocity, as near the convex wall at the bend entrance, will lead to a reduction in the production of kinetic energy as per Eq. (3), whereas a negative gradient of the streamwise velocity, as near the concave wall, will result in an enhancement of the production rate. Thus, the exact production terms in the stress models are able to provide correct response to the streamwise velocity gradients. However, the second term in Eq. (2), being always positive, will always increase turbulence even in case of flow acceleration, and thus it is a poor representation of the response of turbulence to such irrotational straining. The significant overprediction of turbulence near the convex wall by the k-ε model (Figs. 4b and 4c) can be largely attributed to this deficiency. This deficiency is also responsible for the well-known problem of the standard k-ε model, namely, the overprediction of turbulence energy near the stagnation point region.

The major features of the flow at $\theta = 90$ deg (Fig. 4) are similar to those observed at $\theta = 30$ deg. The predicted mean velocity profiles show very thin boundary layers near the convex wall, with the RSM prediction in closest agreement with the data (Fig. 4a). Near the concave wall, strong turbulent mixing brings high-momentum fluid towards the wall, creating a full velocity profile. The RSM model predicts the highest level of turbulence amplification and hence fullest velocity profile near the concave wall. The performance of the ARSM for the convex curvature is similar to that of the NL k-ε model, but it is superior for the concave curvature.

The RSM captures the trend on the effect of concave curvature on the turbulence but underpredicts its magnitude (Figs. 4b and 4c). This can be mainly attributed to the fundamental difference in convex and concave curvature effects. As reported by Muck et al.,[23] Hoffman et al.,[24] Gillis and Johnston,[25] and Barlow and Johnston,[3] the convex curvature mainly attenuates the pre-existing turbulent eddies, whereas the concave curvature may involve both the reorganization of the pre-existing eddy structures and the creation of new large-scale eddies.

As argued by many investigators, a concave curved flow is complex due to possible existence of Taylor–Gortler vortices. However, these vortices have not been observed in many of the experiments.[3] Barlow and Johnston[3] conclude that large scales in concave boundary layers exhibit a range of behaviors from longitudinal vortices (Taylor–Gortler vortices), when upstream nonuniformities are large, to short randomly distributed roll cells (radial inflows and outflows), when the upstream boundary layer is uniform in the mean. Other researchers[1] also suggest that spanwise variations in some experiments are likely to be caused by the nonuniformities in upstream flow. Barlow and Johnston[3] found that the large scales in concave flows are larger than typical large eddies in a flat boundary layer and are more energetic, particularly with regard to fluctuations normal to the wall. Both Monson et al.[6] and Sandborn and Shin[5] have observed energetic large-scale eddies rather than longitudinal vortices near the concave wall. Thus, current underprediction of turbulence enhancement can be attributed mainly to the inability of the models (particularly the standard ε equation) to account for the new large-scale eddy structures in concave curved flows. This is confirmed in the analysis by Luo and Lakshminarayana.[26]

Mean Velocity and Turbulence Properties Downstream of the 180-deg Bend

The flow encounters an adverse pressure gradient on the inner wall and a favorable pressure gradient on the outer wall downstream of $\theta = 90$ deg. Because of the severe adverse pressure gradient, as well as highly diminished turbulent shear stress, the boundary layer separates around $\theta = 150$ deg on the inner wall. The predictions at $\theta = 180$ deg are shown in Fig. 5. The standard k-ε model predicts too small a separation bubble. This is because the separation is hindered by the excessive level of turbulence near the inner wall predicted by the model. The predicted extent of separation is inversely proportional to the predicted level of turbulence near the

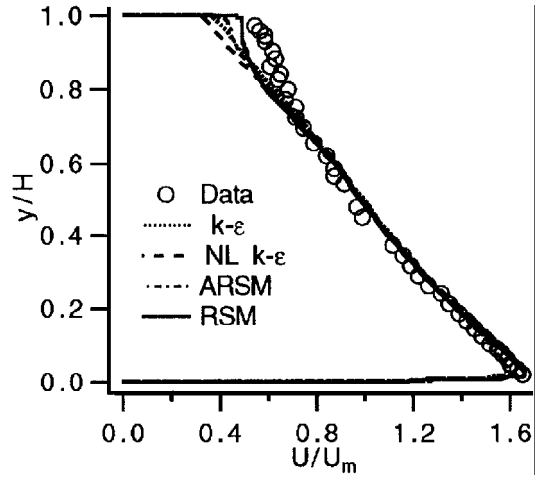

a) Longitudinal velocity

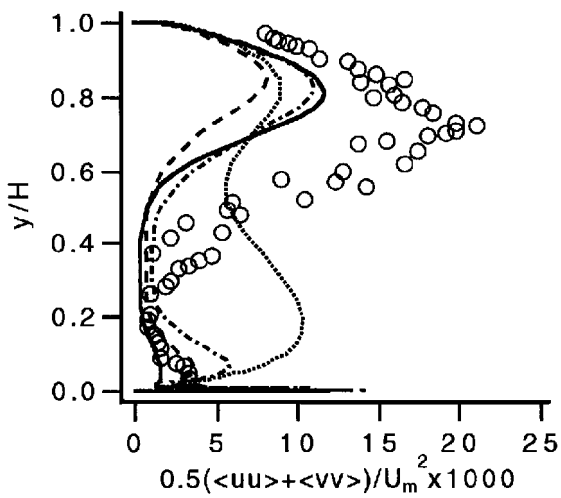

b) Turbulent kinetic energy

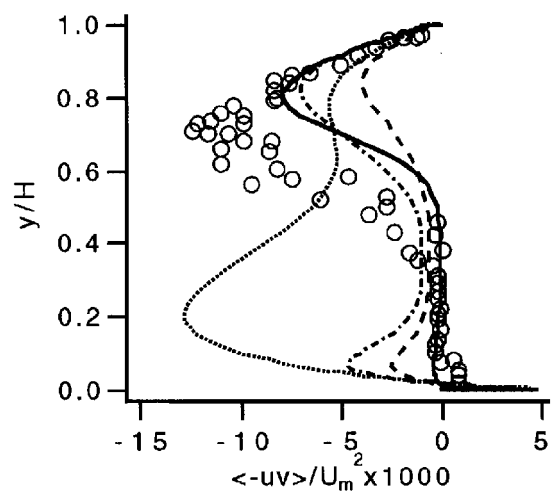

c) Turbulent shear stress

Fig. 4 Profiles at $\theta = 90$ deg (data by Monson et al.,[6] $Re = 1 \times 10^6$).

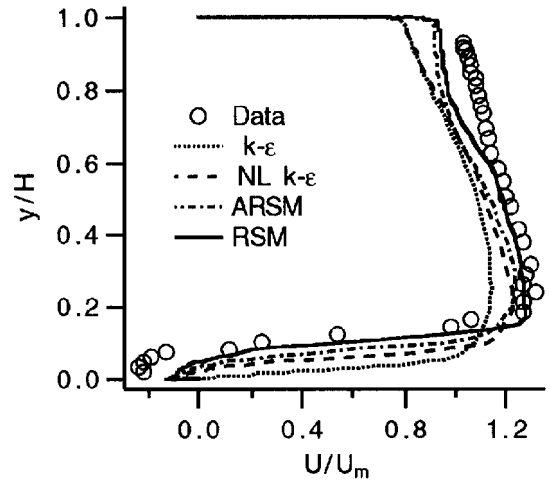

a) Longitudinal velocity

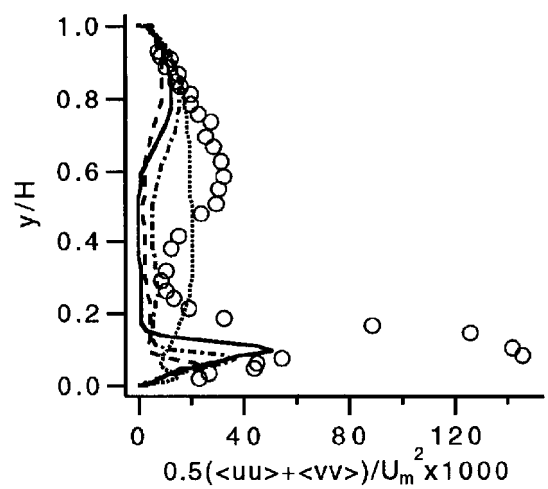

b) Turbulent kinetic energy

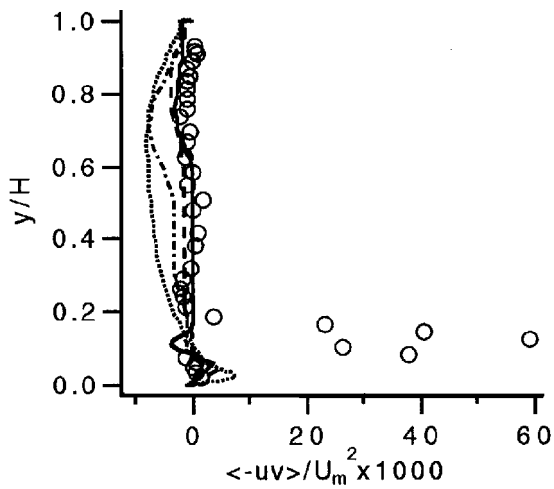

c) Turbulent shear stress

Fig. 5 Profiles at $\theta = 180$ deg (data by Monson et al.,[6] $Re = 1 \times 10^6$).

convex wall upstream of the separation. The RSM model predicts the lowest turbulent energy and shear stress near the convex wall, hence the largest separation bubble downstream, both being in best agreement with the data. The ARSM and the NL k-ε model also capture the major attenuation of turbulence near the convex wall as seen earlier and thus predict larger separation than the k-ε model.

The longitudinal velocity profile across the channel is dominated by both the size of the separation bubble near the inner wall and the amplification of turbulence near the outer wall. The velocity profile predicted by the RSM model is in best agreement with the data because this model provides the best predictions for the features near both walls. The data show a spike in the turbulence profile at the separating streamline, which is not captured by any model. This large value probably results from large unsteadiness of the separation bubble, as reported in Monson et al.[6] Note that turbulent kinetic energy is generated primarily by the large shear strain of flow just outside the separation bubble. This can be seen from the locations of the maximum value of turbulent energy, which are outside the separation bubble and are the locations where the velocity profile has the largest gradient. For the RSM prediction, the peak value of $\frac{1}{2}(\langle uu \rangle + \langle vv \rangle)$ is at $y/H = 0.10$, whereas the height of the separation bubble is about $0.05H$ (Figs. 5a and 5b). The turbulence energy

Table 1 Extent of separation (Monson et al.,[6] $Re = 1 \times 10^6$)

Model/exp.	Separation, θ, deg	Reattachment, x/H
k-ε	172	0.72
NL k-ε	163	1.30
ARSM	157	1.62
RSM	147	1.55
Data	150	1.0–1.5

inside the bubble is supplied primarily by the diffusion across the dividing streamline of the bubble.

At $x = 2H$, both the measurement and the predictions indicate that the flow has reattached, as seen in Fig. 6. The predicted velocity profiles by the RSM are still slowly recovering from separation. The too slow recovery rate after reattachment is a major deficiency of the stress model, as discussed by Leschziner.[20] Near the inner wall, the RSM prediction is inferior to the k-ε prediction, but this is caused by the much larger displacement and associated near-wall wake predicted by the RSM, which are due to the more extensive separation observed earlier. In fact, it should be concluded that all of the models underpredict the rate of recovery. The velocity profiles predicted by the ARSM and the NL k-ε model lie between those from the k-ε model and the RSM.

The levels of turbulent energy and shear stress predicted by the models after reattachment are seen to be proportional to the extent of separation. This is because turbulence is generated primarily by the large shear rate of flow just outside the separation bubble, as stated earlier. The larger separation bubble means a larger shear rate outside the bubble (Fig. 5a) and hence a higher turbulence generation rate. The RSM model predicts the largest separation earlier and hence the highest turbulent energy and shear stress, which are in closest agreement with the data. The k-ε model returns the lowest level of turbulence, consistent with the smallest separation bubble observed earlier.

Wall Static Pressure and Skin-Friction Coefficients

The predicted skin-friction coefficient on the inner wall of the Monson et al.[6] duct is shown in Fig. 7a. The predicted values of C_f from all of the models are almost the same in the flow-acceleration region of the inner wall (from about $x = -0.5H$ to $\theta = 90$ deg, i.e., $S/H = -0.5$ to 1.57). This is because the mean flow is dominated by a large favorable pressure gradient and hence C_f is not sensitive to the predicted level of turbulence in the outer layer of the boundary layer. Once the flow begins to decelerate, the effect of turbulence shear stress becomes important. The RSM predicts the lowest level of turbulence and hence the lowest C_f. The predicted locations of separation inception and reattachment by all of the models are given in Table 1, where the measured reattachment point is in the range of $1.0H$–$1.5H$. All of the three anisotropic models provide more extensive separation than the k-ε model. As discussed earlier, the rate of recovery after reattachment is predicted slower than the measured value, which can also be seen from the slow recovery of C_f along the inner wall.

The skin-friction coefficient on the outer wall is plotted in Fig. 7b, where the data inside the bend are not available. The value of C_f drops as the flow decelerates towards the bend. Inside the bend, the flow is subject to strong concave curvature effects and adverse to a favorable pressure gradient. The levels of C_f predicted by different models are seen to be proportional to the predicted levels of turbulent energy and shear stress near the concave wall (Fig. 4). The RSM and the ARSM provide the best predictions of the amplification of turbulence and hence the best C_f prediction at downstream locations. The C_f inside the bend are probably still underpredicted because the turbulence enhancement has been underestimated by all of the models as observed earlier.

The static pressure coefficients C_p on both inner and outer walls are shown in Fig. 8. The wall static pressure distribution and the pressure loss are largely determined by the extent of separation, which dictates the effective through-flow area and hence the pressure recovery characteristics. The pressure loss through the bend is underpredicted by the k-ε model due to the underprediction of the size of the separation bubble. The NL k-ε prediction is much better near the bend exit because it predicts more extensive separation. The RSM provides the best prediction for the pressure loss far downstream. But the prediction of C_p by this model near the bend exit is not accurate because it predicts too slow a recovery after reattachment. The prediction by the ARSM seems to be a good compromise between those from the k-ε model and the RSM.

Additional Simulations for Effect of δ/R

The preceding results and discussion indicate that the RSM is capable of capturing major features of the highly curved 180-deg duct flow. Since the value of δ/R is an important parameter for the

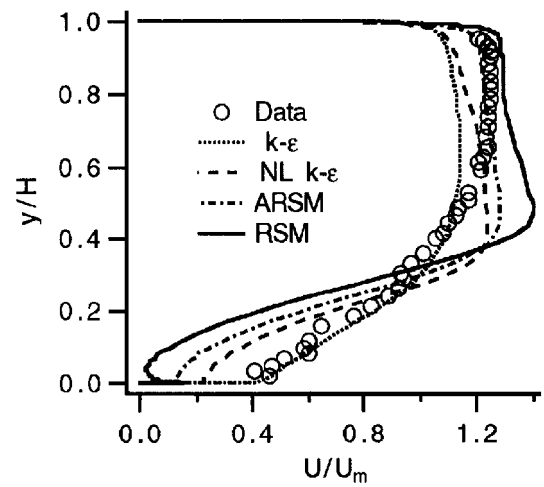

a) Longitudinal velocity

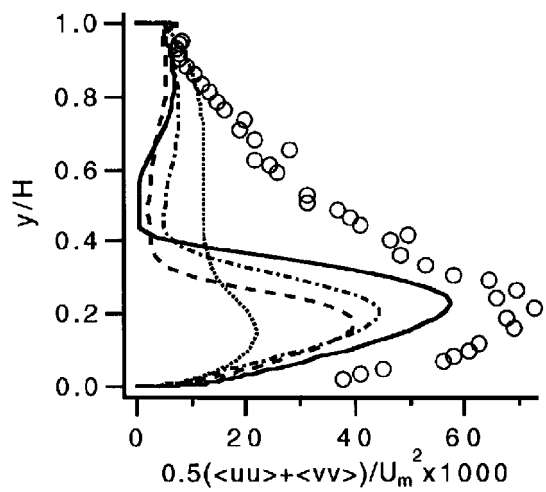

b) Turbulent kinetic energy

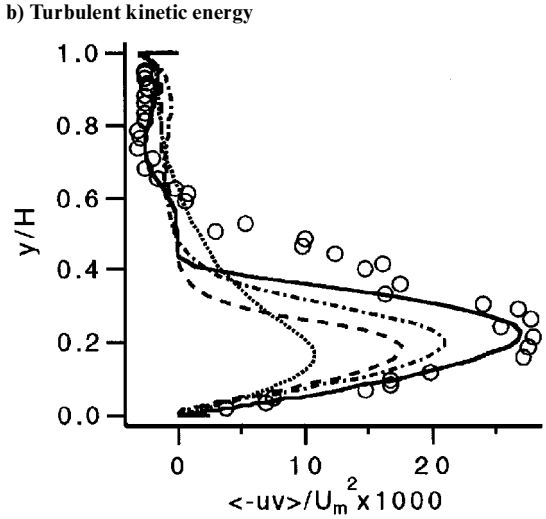

c) Turbulent shear stress

Fig. 6 Profiles at $x = 2H$ (data by Monson et al.,[6] $Re = 1 \times 10^6$).

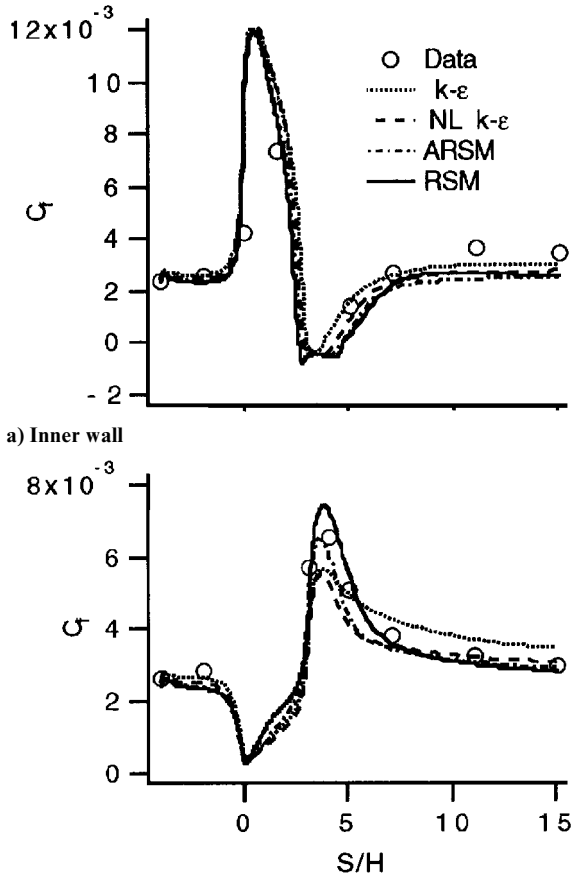

a) Inner wall

b) Outer wall

Fig. 7 Skin-friction coefficients on inner and outer walls (data by Monson et al.,[6] $Re = 1 \times 10^6$).

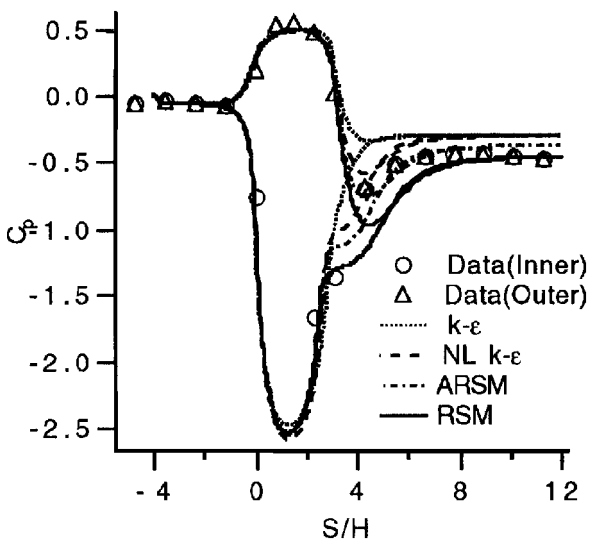

Fig. 8 Wall static pressure coefficients (data by Monson et al.,[6] $Re = 1 \times 10^6$).

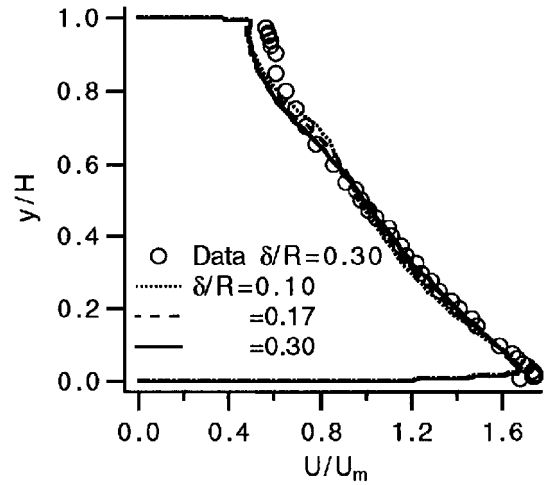

a) Longitudinal velocity

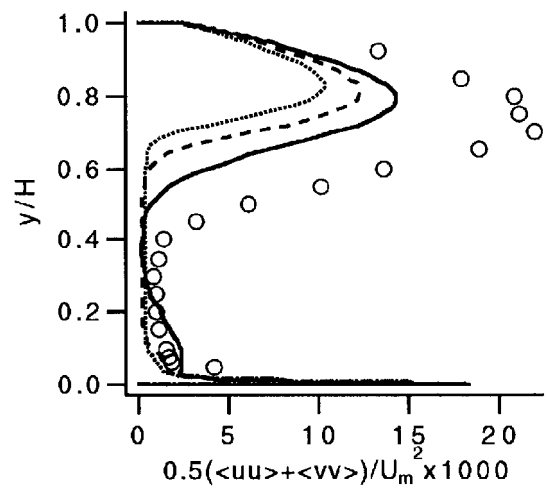

b) Turbulent kinetic energy

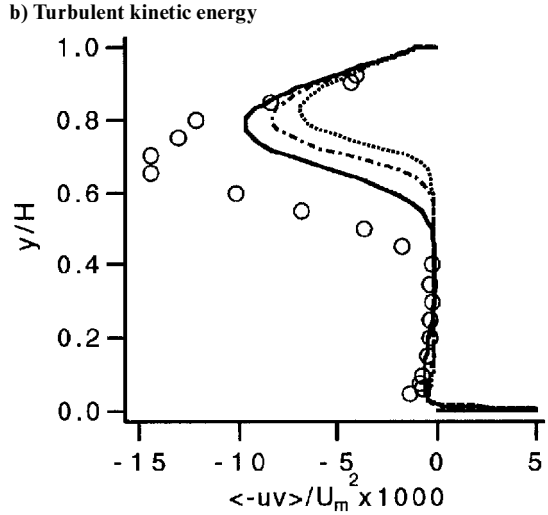

c) Turbulent shear stress

Fig. 9 Profiles at $\theta = 90$ deg (data by Sandborn and Shin,[5] $Re = 2.2 \times 10^5$).

magnitude of curvature effects, additional numerical simulations have been carried out with the RSM to study the effects of δ/R on the development of flow inside the bend and downstream. As stated earlier, $(\delta/R)_{\text{inner}} \approx 1.0$ for the inner wall and $(\delta/R)_{\text{outer}} \approx 0.3$ for the outer wall in the Sandborn and Shin[5] case. Two additional cases (numerical simulations only) with $(\delta/R)_{\text{outer}} \approx 0.17$ and 0.1 have been computed at the same Reynolds number. The corresponding $(\delta/R)_{\text{inner}} \approx 0.5$ and 0.3, respectively.

The predicted profiles at $\theta = 90$ deg are shown in Fig. 9, where the $(\delta/R)_{\text{outer}}$ are used to identify the cases. The turbulence properties near the convex wall are seen to be insensitive to the specific value of δ/R because the turbulence there (Figs. 9b and 9c) has been attenuated to a very low level for all of the cases. This is similiar to the Gillis and Johnston[25] observation that the effect of δ/R is small with $\delta/R > 0.05$ for zero-pressure-gradient flows over convex surface. On the concave side, however, the turbulent energy and shear stress are seen to increase monotonically with the increase in δ/R.

The difference in the response of turbulence, near the convex and concave walls, to the variation of δ/R can be attributed to the major difference in these two opposite curvature effects. There seems to be a low limit for the convex curvature effect, namely, the total damping

of turbulence. However, a corresponding high limit for the concave curvature effect has not been observed. It is likely that the turbulence near the concave wall may further increase with an increase in δ/R as suggested in Figs. 9b and 9c.

The profiles of streamwise velocity (Fig. 9a) are seen to be similar for all values of δ/R. This indicates that the velocity profile inside the bend is largely insensitive to the upstream inflow conditions, which is consistent with the observation by Sandborn and Shin.[5] Downstream at $\theta = 180$ deg, the predicted mean velocity profiles are also close for all of the cases,[10] which suggests that the inflow conditions (thickness of upstream turbulent boundary layer) have negligible influence on the downstream flow separation for strongly curved turnaround duct flows.

Concluding Remarks

A Navier–Stokes procedure, incorporating Reynolds stress models, has been developed based on the four-stage Runge–Kutta scheme. The turbulent flow in a strongly curved 180-deg duct is computed using the RSM, the ARSM, the NL k-ε model, and the k-ε model. The RSM provides the best predictions for major features of this highly curved duct flow, including strong enhancement of turbulence near the concave wall, large reduction of turbulence near the convex wall, and the subsequent separation downstream of the convex wall. It is observed that, to capture the extent of the downstream separation bubble, large reduction of turbulence near the convex wall must be predicted accurately.

The modeling of the concave curvature effect appears to be quite different from the modeling of the convex curvature effect. The RSM is very successful in predicting the turbulence damping but still underpredicts the magnitude of turbulence amplification. The ARSM yields predictions close to those by the RSM. The ARSM predictions are much better than those by the k-ε model. The NL k-ε predictions for convex curvature effect and downstream separation are significantly better than those by the k-ε model. This NL k-ε model predicts reduced turbulence near the concave wall, however. It is thus inferior to the ARSM for modeling concave curvature effects. All of the models predict too slow a recovery after reattachment, indicating that further efforts are needed to improve the modeling of turbulent diffusion, dissipation, and pressure–strain correlation. It should be remarked here that the flow downstream of separation is not likely to be two-dimensional or steady. Most separated flows are three-dimensional and unsteady. Hence these effects may account for some of the discrepancy between the predictions and the data.

Simulation studies with the RSM indicate that the mean flow inside the bend is nearly insensitive to the upstream inflow conditions. The variation of δ/R has more pronounced influence on the turbulence amplification near the concave wall than on the turbulence damping near the convex wall.

Acknowledgments

This work was supported by NASA through Contract NAS 8-38867 monitored by Lisa Griffin of the NASA Marshall Space Flight Center (MSFC). The authors wish to acknowledge NASA for providing the supercomputing resources at MSFC.

References

[1]Bradshaw, P., "Effects of Streamline Curvature on Turbulent Flow," AGARDograph 169, Aug. 1973.

[2]So, R. M. C., and Mellor, G., "Experiment on Convex Curvature Effects in Turbulent Boundary Layers," *Journal of Fluid Mechanics*, Vol. 60, Aug. 1973, p. 43.

[3]Barlow, R. S., and Johnston, J. P., "Structure of a Turbulent Boundary Layer on a Concave Surface," *Journal of Fluid Mechanics*, Vol. 191, 1988, p. 137.

[4]Gibson, M. M., Jones, W. P., and Younis, B. A., "Calculation of Turbulent Boundary Layers on Curved Surfaces," *Physics of Fluids*, Vol. 24, March 1981, p. 386.

[5]Sandborn, V. A., and Shin, J. C., "Water Flow Measurements in a 180 Degree Turn-Around Duct," NASA Marshall Space Flight Center, Contract Rept., June 1989.

[6]Monson, D. J., Seegmiller, H. L., McConnaughey, P. K., and Chen, Y. S., "Comparison of Experiment with Calculations Using Curvature-Corrected Zero and Two Equation Turbulence Models for a Two-Dimensional U-Duct," AIAA Paper 90-1484, June 1990.

[7]Avva, R., Smith, C., and Singhal, A., "Comparative Study of High and Low Reynolds Number Versions of k-ε Models," AIAA Paper 90-0246, Jan. 1990.

[8]Gallardo, J. F., and Lakshminarayana, B., "Computation of Curved Flows Using a Modified k-ε Model of Turbulence Based on Algebraic Reynolds Stress Relations," AIAA Paper 93-0202, Jan. 1993.

[9]Shih, T. H., Zhu, J., and Lumley, J. L., "Modeling of Wall-Bounded Complex Flows and Free Shear Flows," NASA TM 106513, ICOMP-94-3, Feb. 1994.

[10]Luo, J., and Lakshminarayana, B., "Prediction of Strongly Curved Turbulent Duct Flow with Reynolds Stress Model," AIAA 95-2241, June 1995.

[11]Gibson, M. M., and Launder, B., "Ground Effects on Pressure Fluctuations in the Atmospheric Boundary Layer," *Journal of Fluid Mechanics*, Vol. 86, 1978, p. 491.

[12]Lien, F. S., and Leschziner, M. A., "Assessment of Turbulence-Transport Models Including Non-Linear RNG Eddy-Viscosity Formulation and Second-Moment Closure for Flow over a Backward-Facing Step," *Computers and Fluids*, Vol. 23, No. 8, 1994, pp. 983–1004.

[13]Rodi, W., "A New Algebraic Relation for Calculating Reynolds Stress," *ZAMM*, Vol. 56, 1976, pp. 219–222.

[14]Launder, B. E., and Spalding, D. B., "The Numerical Computation of Turbulent Flows," *Computer Methods in Applied Mechanics and Engineering*, Vol. 3, 1974, pp. 269–289.

[15]Lakshminarayana, B., "Turbulence Modelling for Complex Shear Flows," *AIAA Journal*, Vol. 24, No. 12, 1986, pp. 1900–1917.

[16]Shih, T.-H., Zhu, J., and Lumley, J. L., "A Realizable Reynolds Stress Algebraic Equation Model," NASA TM 105993, 1993.

[17]Wolfshtein, M., "The Velocity and Temperature Distribution in One-Dimensional Flow with Turbulence Augmentation and Pressure Gradient," *International Journal of Heat and Mass Transfer*, Vol. 12, 1969, pp. 301–318.

[18]Chen, H. C., and Patel, V. C., "Near-Wall Turbulence Models for Complex Flows Including Separation," *AIAA Journal*, Vol. 26, 1988, pp. 641–648.

[19]Kunz, R. F., and Lakshminarayana, B., "Three-Dimensional Navier–Stokes Computation of Turbomachinery Flows Using an Explicit Numerical Procedure and a Coupled k-ε Turbulence Model," *Journal of Turbomachinery*, Vol. 114, July 1992, p. 627.

[20]Leschziner, M. A., "Modelling Engineering Flows with Reynolds Stress Turbulence Closure," *Journal of Wind Engineering and Industrial Aerodynamics*, Vol. 35, 1990, pp. 21–47.

[21]Sotiropoulos, F., and Patel, V. C., "Prediction of Turbulent Flow Through a Transition Duct Using a Second-Moment Closure," *AIAA Journal*, Vol. 32, No. 11, 1994, pp. 2194–2204.

[22]Launder, B. E., Reynolds, W. C., and Rodi, W., *Turbulence Models and Their Applications*, Editions Eyrolles, Paris, France, 1984.

[23]Muck, K. C., Hoffmann, P. H., and Bradshaw, P., "The Effect of Convex Curvature on Turbulent Boundary Layers," *Journal of Fluid Mechanics*, Vol. 161, 1985, p. 347.

[24]Hoffmann, P. H., Muck, K. C., and Bradshaw, P., "The Effect of Concave Surface Curvature on Turbulent Boundary Layers," *Journal of Fluid Mechanics*, Vol. 161, 1985, pp. 371–403.

[25]Gillis, J. C., and Johnston, J. P., "Turbulent Boundary-Layer Flow and Structure on a Convex Wall and Its Redevelopment on a Flat Wall," *Journal of Fluid Mechanics*, Vol. 135, 1983, p. 123.

[26]Luo, J., and Lakshminarayana, B., "Analysis of Streamline Curvature Effects on Wall-Bounded Turbulent Flows," 3rd International Symposium on Engineering Turbulence Modeling and Measurements, Crete, Greece, May 1996.